International Journal of Engineering Science 130 (2018) 51–61

Contents lists available at ScienceDirect

International Journal of Engineering Science

journal homepage: www.elsevier.com/locate/ijengsci

Elastic instabilities and shear waves in hyperelastic composites with various periodic fiber arrangements

Pavel I. Galich[a], Viacheslav Slesarenko[a], Jian Li[a], Stephan Rudykh[b,*]

[a] *Faculty of Aerospace Engineering, Technion – Israel Institute of Technology, Haifa 32000, Israel*
[b] *Department of Mechanical Engineering, University of Wisconsin – Madison, Madison, WI 53706, United States*

ARTICLE INFO

Article history:
Received 20 January 2018
Revised 28 April 2018
Accepted 20 May 2018
Available online 31 May 2018

Keywords:
Fiber composites
Instabilities
Finite deformations
Wave propagation
Dispersion

ABSTRACT

We investigate the influence of fiber arrangement on elastic instabilities and shear wave propagation in hyperelastic 3D fiber composites (FCs) with periodic rectangular arrays of cylindrical fibers. We show that elastic instabilities and shear waves propagating along the fibers in uniaxially deformed FCs can be tuned through the choice of the periodicity of fiber arrangements (or periodic unit cell aspect ratio b/a) of FCs. In particular, we find that the range of deformations, where FCs are mechanically stable, decreases with an increase in the periodicity aspect ratio. Moreover, we identify the bounds for the critical stretches in FCs with periodic rectangular arrays of fibers. We find that the FC critical stretches are bounded by the critical values for corresponding 3D laminates (upper bound) and FCs with square arrays of fibers (lower bound). In FCs with large volume fractions of fibers (e.g. 25%), the polarization directions of the long shear waves start rotating upon approaching critical deformation. This indicates that fibers develop buckling shapes in non-principal planes. In FCs with small volume fractions of fibers (e.g. 5%), polarizations of the shear waves (of the lowest frequencies) barely changes the direction upon attaining the critical deformation; hence, buckling of fibers initially develops in one of the principal planes, depending on the periodicity aspect ratio of FCs.

1. Introduction

Soft fiber-reinforced composites (FCs), simultaneously possessing high strength, lightweight, and flexibility, are widely present in nature (Saheb & Jog, 1999). However, natural materials cannot provide all the desirable in industry properties because of biodegradability and poor resistance to moisture or ultraviolet; therefore, synthetic composites are of great interest (Beloshenko, Voznyak, Voznyak, & Savchenko, 2017). An advantage of soft (nonlinear) composites over hard (linear) composites is high elasticity, allowing significant reversible geometry changes (including buckling Andrianov, Kalamkarov, & Weichert, 2012; Gao & Li, 2017; Li, Kaynia, Rudykh, & Boyce, 2013; Parnes & Chiskis, 2002); consequently, their effective properties can be tuned by elastic deformation. In particular, elastic waves in soft composites can be controlled by deformation (Bertoldi & Boyce, 2008; Galich, Fang, Boyce, & Rudykh, 2017; Galich & Rudykh, 2017; Slesarenko, Galich, & Rudykh, 2018; Nam, Merodio, Ogden, & Vinh, 2016). It is worth noting also that many soft biological tissues are found to possess fiber-matrix microstructures (Humphrey, 2002), and the soft tissues frequently experience large deformations due to different physiological processes. Hence, investigation of elastic wave propagation and instabilities (that can significantly influence

* Corresponding author.
E-mail addresses: rudykh@wisc.edu, rudykh@mit.edu (S. Rudykh).

https://doi.org/10.1016/j.ijengsci.2018.05.003
0020-7225/© 2018 Elsevier Ltd. All rights reserved.

elastic waves) in 3D fiber-reinforced composites undergoing finite deformations can be beneficial for biomedical applications such as ultrasound testing.

By employing the nonlinear elastic theory (Truesdell & Noll, 1965) and a phenomenological approach, Scott and Hayes (1976) considered small amplitude plane waves superimposed on a homogeneous deformation in the so-called idealized fiber-reinforced materials, assuming incompressibility of the matrix and inextensibility of the fibers. Later, Scott (1991, 1992), and Rogerson and Scott (1994) extended this analysis for a broader class of finitely deformed fiber-reinforced materials with marginally extensible and compressible constituents. Recently, Ogden and Singh (2011) exploited a phenomenological theory of invariants and presented a more general and transparent formulation of the theory for small amplitude waves propagating in deformed transversely isotropic hyperelastic solids. This approach was successfully utilized for calculating speeds of homogeneous plane waves (Vinh & Merodio, 2013) and non-principal Rayleigh waves (Nam, Merodio, & Vinh, 2016; Vinh, Merodio, Hue, & Nam, 2014) in various deformed transversely isotropic incompressible solids. More recently, Galich, Slesarenko, and Rudykh (2017) employed a micromechanics based approach (deBotton, Hariton, & Socolsky, 2006) and derived explicit closed form expressions for phase and group velocities of shear waves propagating in finitely deformed 3D FCs. By application of the Bloch–Floquet approach in the finite element code (Aberg & Gudmundson, 1997; Bertoldi & Boyce, 2008), Galich, Slesarenko et al. (2017) also investigated dispersion of shear waves propagating along the fibers in finitely deformed FCs with square arrays of fibers. However, the influence of fiber arrangement on shear wave propagation in finitely deformed 3D FCs has not been investigated.

In this paper, we investigate the influence of fiber arrangement on small amplitude shear wave propagation in finitely deformed FCs with rectangular arrays of cylindrical fibers. We limit our consideration of the applied finite deformation prior to the onset of elastic instabilities. Recall that elastic instabilities in hyperelastic FCs may develop according to the microscopic or macroscopic scenarios depending on the material composition (Slesarenko & Rudykh, 2017; Triantafyllidis & Maker, 1985). In particular, the conditions for the onset of macroscopic instabilities, characterized by wavelengths significantly larger than the characteristic microstructure size, can be predicted by evaluation of the homogenized tensor of elastic moduli that can be obtained from phenomenological (Merodio & Ogden, 2002; Merodio & Pence, 2001; Qiu & Pence, 1997) or micromechanics based (Agoras, Lopez-Pamies, & Castañeda, 2009; Lopez-Pamies & Castañeda, 2006a; 2006b; Rudykh & deBotton, 2012) material models for transversely isotropic FCs. The conditions for the onset of microscopic instabilities, characterized by wavelengths comparable with the characteristic microstructure size, can be predicted by the Bloch–Floquet analysis (Geymonat, Müller, & Triantafyllidis, 1993; Michel, Lopez-Pamies, Ponte Castañeda, & Triantafyllidis, 2010; Nestorovic & Triantafyllidis, 2004; Slesarenko & Rudykh, 2017; Triantafyllidis, Nestorovic, & Schraad, 2006). However, for uniaxially compressed 3D FCs with rectangular arrays of fibers, dependence of the critical stretches and wavelengths on fiber arrangement has not been discussed in literature. Here, we specifically focus on the influence of fiber arrangement, and we identify the conditions leading to the macroscopic/microscopic instabilities in hyperelastic FCs with rectangular arrays subjected to compressive deformations along the fibers. We show that the critical stretches for FCs with rectangular arrays of fibers are bounded by the corresponding critical values for the 3D laminates and FCs with square arrays of fibers. Remarkably, this holds true regardless of the volume fraction of fibers and contrast in shear moduli between the fibers and matrix. Next, we study the dispersion curves of shear waves in FCs deformed close to the instability point, where the most remarkable behavior of shear waves is observed. We observe that the polarization vectors of long shear waves propagating along the fibers in FCs with large volume fractions of fibers (e.g. 25%) rotate upon attaining the critical deformation level. These changes in direction of polarization indicate that fibers develop buckling shapes in non-principal planes. Moreover, polarizations of the lowest frequency shear waves in FCs with small fiber volume fractions (e.g. 5%) change their directions depending on the aspect ratio of the FC arrays. Thus, the buckling shapes can be tailored through the choice of the FC array aspect ratio.

2. Theoretical background

Consider a continuum body and identify each point in the reference (undeformed) configuration with vector $\mathbf{X}$. In the current (deformed) configuration, the new location of the corresponding points is defined by vector $\mathbf{x} = \mathbf{x}(\mathbf{X}, t)$. Then, the deformation gradient is $\mathbf{F} = \partial\mathbf{x}/\partial\mathbf{X}$, and $J \equiv \det\mathbf{F} > 0$. For a hyperelastic compressible material with a strain energy function $\psi(\mathbf{F})$, the first Piola–Kirchhoff stress tensor can be calculated as follows

$$\mathbf{P} = \frac{\partial\psi(\mathbf{F})}{\partial\mathbf{F}}. \tag{1}$$

For an incompressible material, $J = 1$ and Eq. (1) modifies as

$$\mathbf{P} = \frac{\partial\psi(\mathbf{F})}{\partial\mathbf{F}} - p\mathbf{F}^{-T}, \tag{2}$$

where p represents an unknown Lagrange multiplier. The corresponding Cauchy stress tensor is related to the first Piola–Kirchhoff stress tensor via the relation $\boldsymbol{\sigma} = J^{-1}\mathbf{P}\cdot\mathbf{F}^T$.

In the absence of body forces the equations of motion can be written in the undeformed configuration as

$$\mathrm{Div}\mathbf{P} = \rho_0\frac{D^2\mathbf{x}}{Dt^2}, \tag{3}$$

where ρ_0 is the initial density of the material and the operator $D^2(\bullet)/Dt^2$ represents the material time derivative. If the deformation is applied quasi-statically, the right hand part of (3) can be assumed to be zero, and the equilibrium equation is obtained as

$$\mathrm{Div}\mathbf{P} = \mathbf{0}. \tag{4}$$

Consider next infinitesimal motions superimposed on the equilibrium state. The equations of the incremental motions are

$$\mathrm{Div}\dot{\mathbf{P}} = \rho_0 \frac{D^2\mathbf{u}}{Dt^2}, \tag{5}$$

where $\dot{\mathbf{P}}$ is the incremental change in the first Piola–Kirchhoff stress tensor and $\mathbf{u}$ is the incremental displacement.

The linearized constitutive law can be written as

$$\dot{P}_{ij} = \mathcal{A}_{0ijkl}\dot{F}_{kl}, \tag{6}$$

where $\dot{\mathbf{F}} = \mathrm{Grad}\ \mathbf{u}$ is the incremental change in the deformation gradient, and the tensor of elastic moduli is defined as $\mathcal{A}_{0i\alpha k\beta} = \partial^2\psi/\partial F_{i\alpha}\partial F_{k\beta}$. Under substitution of (6) into (5) the incremental motion equation takes the form

$$\mathcal{A}_{0ijkl}u_{k,lj} = \rho_0 \frac{D^2u_i}{Dt^2}. \tag{7}$$

2.1. Small amplitude motions superimposed on large deformations

To analyze small amplitude motions superimposed on a finite deformation, we present equation of motion (7) in the updated Lagrangian formulation

$$\mathcal{A}_{ijkl}u_{k,lj} = \rho \frac{\partial^2u_i}{\partial t^2}, \tag{8}$$

where $\mathcal{A}_{iqkp} = J^{-1}\mathcal{A}_{0ijkl}F_{pl}F_{qj}$ is the updated tensor of elastic moduli and $\rho = J^{-1}\rho_0$ is the density of the deformed material.

We seek a solution for Eq. (8) in the form of plane waves with constant polarization

$$\mathbf{u} = \mathbf{g}h(\mathbf{n}\cdot\mathbf{x} - ct), \tag{9}$$

where h is a twice continuously differentiable function and unit vector $\mathbf{g}$ denotes the polarization; the unit vector $\mathbf{n}$ defines the direction of wave propagation, and c is the phase velocity of the wave.

Substituting (9) into (8), we obtain

$$\mathbf{Q}(\mathbf{n})\cdot\mathbf{g} = \rho c^2\mathbf{g}, \tag{10}$$

where

$$Q_{ik} = \mathcal{A}_{ijkl}n_jn_l \tag{11}$$

is the acoustic tensor defining the condition of propagation of the infinitesimal plane waves. Thus, for a real wave to exist acoustic tensor has to be positively defined for any non-zero vectors $\mathbf{n}$ and $\mathbf{g}$

$$\mathbf{g}\cdot\mathbf{Q}(\mathbf{n})\cdot\mathbf{g} = \mathcal{A}_{ijkl}n_jn_lg_ig_k = \rho c^2 > 0. \tag{12}$$

Recall that the inequality

$$\mathcal{A}_{ijkl}n_jn_lg_ig_k > 0 \tag{13}$$

is called the strong ellipticity condition (Truesdell & Noll, 1965). This inequality also arises in the stability theory of elastic and elasto-plastic solids. Thus, if the inequality (13) does not hold true in any point of the body for the applied boundary conditions, the body is unstable in this state. In a similar vein, the body becomes unstable if the velocity of at least one wave with any polarization and any propagation direction in this body becomes zero. It is worth noting that loss of strong ellipticity analysis is widely used for finding macroscopic instabilities in homogenizable composites (Agoras et al., 2009; Lopez-Pamies & Castañeda, 2006a; 2006b; Rudykh & deBotton, 2012).

For incompressible materials Eq. (8) modifies as

$$\mathcal{A}_{ijkl}u_{k,lj} + \dot{p}_{,i} = \rho \frac{\partial^2u_i}{\partial t^2}, \tag{14}$$

together with the incompressibility constraint

$$u_{i,i} = 0. \tag{15}$$

Substitution of (9) and $\dot{p} = p_0h'(\mathbf{n}\cdot\mathbf{x} - ct)$, where p_0 is a scalar, into (14) and (15) yields

$$\hat{\mathbf{Q}}(\mathbf{n})\cdot\mathbf{g} = \rho c^2\mathbf{g} \quad \text{and} \quad \mathbf{g}\cdot\mathbf{n} = 0, \tag{16}$$

where $\hat{\mathbf{Q}} = \hat{\mathbf{I}}\cdot\mathbf{Q}\cdot\hat{\mathbf{I}}$ and $\hat{\mathbf{I}} = \mathbf{I} - \mathbf{n}\otimes\mathbf{n}$ is the projection onto the plane normal to $\mathbf{n}$. Thus, in the incompressible case, the strong ellipticity condition (13) subject to the restriction $\mathbf{g}\cdot\mathbf{n} = 0$.

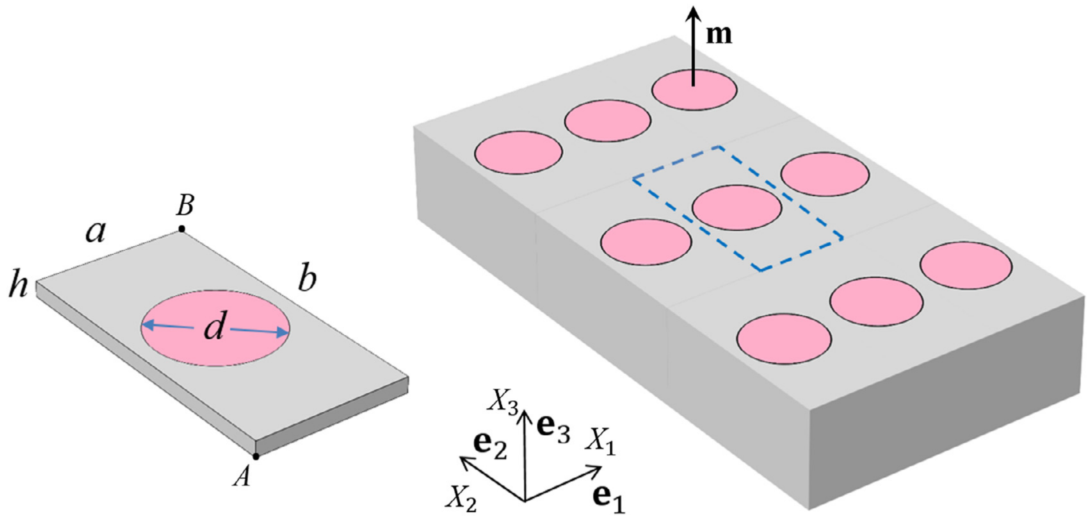

Fig. 1. RVE for a 3D periodic FC with a rectangular arrangement of fibers, where h denotes the height of the RVE.

3. Problem description

Consider a periodic FC made out of rectangular arrays of aligned cylindrical fibers embedded in a softer matrix with the volume fractions $v_f = \pi d^2/(4ab) < \pi a/(4b)$ and $v_m = 1 - v_f$, where d is the initial diameter of fibers, a and b $(b \geq a)$ are the initial distances between the fibers in two perpendicular directions (see Fig. 1). Here and thereafter, the fields and parameters of the constituents are denoted by the subscripts $(\bullet)_f$ and $(\bullet)_m$ for fibers and matrix, respectively. The perfect bonding between fibers and matrix is assumed; hence,

$$\left(\mathbf{F}_f - \mathbf{F}_m\right) \cdot \mathbf{m} = \mathbf{0} \quad \text{and} \quad \left(\mathbf{P}_f - \mathbf{P}_m\right) \cdot \mathbf{m}_\perp = \mathbf{0}, \tag{17}$$

where the unit vector $\mathbf{m}$ denotes the initial fiber directions ($\mathbf{m} = \mathbf{e}_3$ in Fig. 1), and $\mathbf{m}_\perp$ is the arbitrary unit vector orthogonal to $\mathbf{m}$.

To analyze shear wave propagation in finitely deformed periodic FCs, we superimpose small amplitude motions on a finitely deformed state (Bertoldi & Boyce, 2008). Recall that in a periodic structure plane waves can be described by the Bloch function (Kushwaha, Halevi, Dobrzynski, & Djafari-Rouhani, 1993). To perform the analysis, we utilize the finite element method with the help of COMSOL 5.2a. Fig. 1 shows an example of representative volume element (RVE) for a FC with a rectangular periodic unit cell that occupies a domain Ω in the undeformed configuration, namely

$$-a/2 \leq X_1 \leq a/2, \quad -b/2 \leq X_2 \leq b/2, \quad \text{and} \quad -h/2 \leq X_3 \leq h/2. \tag{18}$$

3.1. Static finite deformation

Firstly, we obtain the solution for the finitely deformed periodic FC. The macroscopic deformation gradient $\bar{\mathbf{F}} = 1/\Omega \int_\Omega \mathbf{F} dV$ is applied through periodic boundary conditions imposed on the displacements of the RVE faces such that

$$\mathbf{U}_B - \mathbf{U}_A = \left(\bar{\mathbf{F}} - \mathbf{I}\right) \cdot (\mathbf{X}_B - \mathbf{X}_A), \tag{19}$$

where A and B are the nodes on the opposite faces of the RVE boundary (see Fig. 1) and $\mathbf{U} = \mathbf{x}(\mathbf{X}) - \mathbf{X}$ is the displacement field. The macroscopic first Piola–Kirchhoff stress tensor and the corresponding Cauchy stress tensor are calculated as $\bar{\mathbf{P}} = 1/\Omega \int_\Omega \mathbf{P} dV$ and $\bar{\boldsymbol{\sigma}} = 1/\Omega \int_\Omega \boldsymbol{\sigma} dV$, respectively. Rigid body motions are prevented by fixing the displacements of a single node, i.e. $\mathbf{U}_A = \mathbf{0}$. Although the analysis is general and it can be applied for materials subject to any macroscopic homogeneous deformation $\bar{\mathbf{F}}$, in this work we subject FCs to uniaxial deformation in 3D setting

$$\bar{\mathbf{F}} = \lambda \mathbf{e}_3 \otimes \mathbf{e}_3 + \lambda^{-1/2} (\mathbf{I} - \mathbf{e}_3 \otimes \mathbf{e}_3), \tag{20}$$

where λ is the macroscopic stretch applied along the fibers and $\mathbf{e}_3$ is the unit basis vector in the direction of fibers.

We describe the behavior of composite constituents with the neo-Hookean strain energy density function integrated in COMSOL 5.2a as

$$\psi_{f,m} = \frac{\mu_{f,m}}{2} (\mathbf{F}_{f,m} : \mathbf{F}_{f,m} - 3) - \mu_{f,m} \ln(\det \mathbf{F}_{f,m}) + \frac{\Lambda_{f,m}}{2} \left(\ln(\det \mathbf{F}_{f,m})\right)^2, \tag{21}$$

where μ is the shear modulus and Λ is the first Lame's parameter. To preserve the nearly incompressible behavior of the constituents, we set a high ratio between the first Lame's parameter and the shear modulus, namely $\Lambda_{f,m}/\mu_{f,m} = 10^3$ in all simulations.

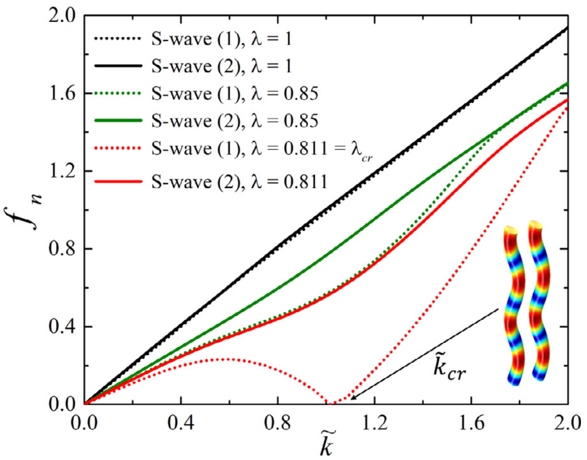

Fig. 2. Evolution of the dispersion curves of the shear waves of the lowest frequencies propagating along the fibers in FC subject to uniaxial compression (20). Example is given for FC with $v_f = 0.05$, $b/a = 10$ and $\mu_f/\mu_m = 15$. $\lambda_{cr} = 0.811$ and $\tilde{k}_{cr} = 1.02$.

3.2. Small-amplitude motions superimposed on a deformed state (Bloch–Floquet approach)

Secondly, we superimpose the Bloch–Floquet periodicity conditions on the deformed state. The corresponding incremental change in the displacement and the first Piola–Kirchhoff stress tensor are

$$\mathbf{u}(\mathbf{X}, t) = \mathcal{U}(\mathbf{X})e^{-i\omega t} \quad \text{and} \quad \dot{\mathbf{P}}(\mathbf{X}, t) = \mathcal{P}(\mathbf{X})e^{-i\omega t}, \tag{22}$$

where ω is the angular frequency. By substitution (22) in (5), we obtain

$$\mathrm{Div}\mathcal{P} + \rho_0\omega^2\mathcal{U} = \mathbf{0}. \tag{23}$$

Next, according to the Floquet theorem

$$\mathcal{U}(\mathbf{X} + \mathbf{R}) = \mathcal{U}(\mathbf{X})e^{-i\mathbf{K}\cdot\mathbf{R}} \quad \text{and} \quad \mathcal{P}(\mathbf{X} + \mathbf{R}) = \mathcal{P}(\mathbf{X})e^{-i\mathbf{K}\cdot\mathbf{R}}, \tag{24}$$

where $\mathbf{R}$ defines the distance between the nodes on the opposite faces of the RVE in the reference configuration. The periodicity conditions (24) are imposed in the finite element code through the corresponding boundary conditions for the displacements of the opposite faces (Bertoldi & Boyce, 2008; Slesarenko & Rudykh, 2017). The dispersion relations are obtained by solving the eigenvalue problem stemming from Eq. (22) to (24) for a range of the wave vectors $\mathbf{K}$. Recall that the corresponding wave vector in the deformed configuration can be found via relation $\mathbf{k} = \mathbf{F}^{-T} \cdot \mathbf{K}$. In this work, we present results for the wave propagation direction along the fibers only, namely $\mathbf{k} = k\mathbf{e}_3$. For completeness, we verified our numerical results against the exact analytical solutions for finitely deformed 3D periodic FCs in the long wave limit (Galich, Slesarenko et al., 2017).

3.3. The implementation of Bloch–Floquet approach for analysis of elastic instabilities in FCs

Fig. 2 illustrates the typical evolution of the dispersion curves of the two shear waves of the lowest frequencies propagating along the fibers in FC subject to uniaxial compression (20), calculated via numerical approach described in above sections. The frequency is normalized as $f_n = \frac{\omega(a+b)}{4\pi}\sqrt{\bar{\rho}_0/\tilde{\mu}}$, where $\tilde{\mu} = \mu_m\left(\left(1 + v_f\right)\mu_f + v_m\mu_m\right)/\left(v_m\mu_f + \left(1 + v_f\right)\mu_m\right)$ and $\bar{\rho}_0 = v_f\rho_f + v_m\rho_m$ is the average density of the FC; the wave vector is normalized as $\tilde{k} = k(a + b)/4\pi = (a + b)/2l$, where l is the wavelength. Here and thereafter, we consider FCs with identical densities of fibers and matrix, namely $\rho_f/\rho_m = 1$.

While dispersion curves of shear waves are linear for the undeformed FCs (see black curves in Fig. 2), they become highly nonlinear upon a subsequent increase in compressive loading, which is clearly visible for stretch ratios $\lambda = 0.85$ (green curves) and $\lambda = 0.811$ (red curves). Eventually, when a critical stretch ratio λ_{cr} is achieved, a zero eigenvalue appears at a specific wavenumber $\tilde{k}_{cr} \neq 0$ (see the red dotted curve in Fig. 2). This critical stretch corresponds to the onset of microscopic instabilities (buckling of fibers), and the value of $\tilde{k}_{cr}$ defines the geometry of the buckling mode. The onset of instability at $\tilde{k}_{cr} \to 0$ corresponds to the long-wave or macroscopic instability. In the numerical simulations this limit is approximately captured by assigning small enough values of $\tilde{k}$. It is worth mentioning that (Geymonat et al., 1993) rigorously demonstrated the equivalence of the macroscopic loss of strong ellipticity and the special case of $\tilde{k}_{cr} \to 0$ in Bloch–Floquet analysis. We note that with the onset of instability, velocity of the shear wave with certain wavenumber (corresponding to the critical wavelength) becomes zero. In case of macroscopic instability, the velocity of long shear waves (with $\tilde{k} \to 0$) become zero.

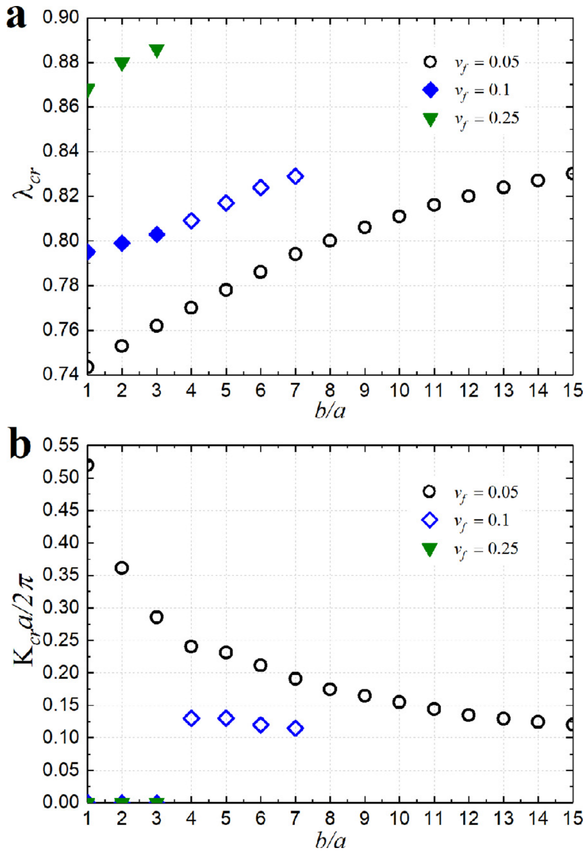

Fig. 3. Dependencies of critical stretch (a) and wavenumber (b) on the aspect ratio of FC with different volume fractions. The hollow and solid symbols correspond to microscopic and macroscopic instabilities, respectively. $\mu_f/\mu_m = 15$.

4. Results and discussion

We start with determining the critical stretches and wavenumbers (or wavelength) corresponding to the onset of elastic instabilities in uniaxially compressed (20) FCs with rectangular arrays of fibers (see Slesarenko & Rudykh, 2017 for the detailed description of the applied Bloch–Floquet method and results for FCs with square arrays of fibers). Next, we analyze the shear wave propagation in the direction of fibers in nearly unstable FCs, where the highly nonlinear dispersion relation is expected. In parallel, by analyzing polarizations of shear waves, we draw some conclusions on the expected buckling shapes of fibers in FCs with rectangular arrays of fibers.

4.1. Elastic instabilities

Fig. 3(a) presents the critical stretches as functions of the aspect ratio for FCs with $\mu_f/\mu_m = 15$ and different volume fractions of the fibers. Clearly, FCs become less stable with an increase in the aspect ratio, regardless of the volume fraction of the fibers. For example, for FCs with $v_f = 0.05$, $b/a = 1$ and $b/a = 15$, the critical stretches are $\lambda_{cr} = 0.744$ and $\lambda_{cr} = 0.830$, respectively. It is known that elastic instabilities in FCs may develop according to the macroscopic (infinite wavelength, i.e. $K_{cr} \to 0$) or microscopic (finite wavelength) scenarios depending on the material composition (Geymonat et al., 1993; Slesarenko & Rudykh, 2017; Triantafyllidis & Maker, 1985). To clarify the transitions between these instability scenarios, Fig. 3(b) shows the critical wavenumbers $K_{cr} = \lambda_{cr}k_{cr}$ as functions of the aspect ratio for FCs with $\mu_f/\mu_m = 15$. Thus, FCs with volume fraction of fibers $v_f = 0.25$ undergo instabilities via macroscopic scenario, regardless of aspect ratio, while FCs with much smaller volume fraction of fibers $v_f = 0.05$ follow the microscopic scenario. However, FCs with moderate amount of fibers $v_f = 0.1$ can develop instabilities either by the macroscopic or microscopic scenarios, depending on the aspect ratio of FC. In particular, FCs with $v_f = 0.1$ and $\mu_f/\mu_m = 15$ lose the stability by the macroscopic scenario for $b/a \leq 3$ and by the microscopic scenario for $b/a \geq 4$ (Fig. 3(b)). The critical wavenumber K_{cr} decreases with an increase in the aspect ratio, when FCs follow the microscopic scenario for instabilities (see hollow symbols in Fig. 3(b)).

According to our calculations, the critical stretches for FCs with rectangular arrays of fibers are bounded by the corresponding critical values for 3D layered composites at the top – they cannot be less stable than 3D layered composites with

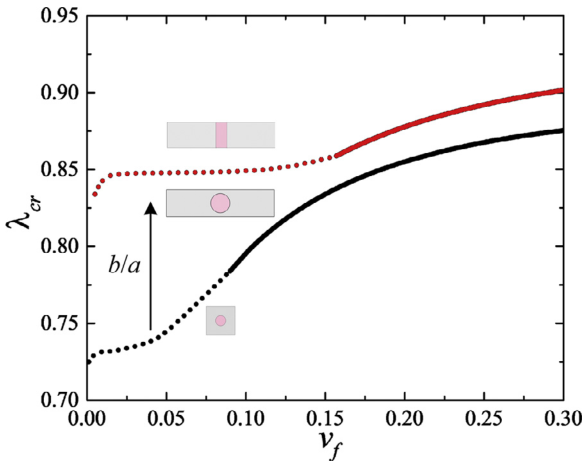

Fig. 4. Limits of critical stretches for the FCs with rectungular arrays of fibers. The top red and bottom black curves reffer to the critical stretches for the uniaxially compressed 3D laminates and FCs with square arrays of fibers, respectively. $\mu_f/\mu_m = 15$. (For interpretation of the references to color in this figure legend, the reader is referred to the web version of this article.)

the same volume fraction of stiffer phase and contrast in shear moduli. Moreover, FCs with rectangular arrays of fibers cannot be more stable than FCs with square arrays of fibers having the identical volume fraction of fibers and contrast in shear moduli. The bounds of critical stretches for the FCs with rectangular arrays of fibers and $\mu_f/\mu_m = 15$ are shown in Fig. 4. The upper bound of the critical stretch (red curve in Fig. 4) for FCs with rectangular arrays of fibers can be explained as a consequence of the changes in geometry of the FC, i.e. FCs with rectangular arrays of fibers geometrically tend to the layered composites as the aspect ratios of FCs increase. Note that the bounds of critical stretches for FCs with $\mu_f/\mu_m = 100$ (i.e. the critical stretches for 3D laminates and FCs with square arrays of fibers) can be found in Slesarenko and Rudykh (2017).

4.2. Shear wave propagation along fibers

Another important question is: what are the buckling shapes of fibers in compressed FCs with rectangular arrays of fibers? Remarkably, the investigation of shear waves of the lowest frequencies in FCs deformed close to the critical point provides useful insights on the expected buckling shapes. In particular, the polarization of the shear wave with velocity approaching zero defines the plane of buckling. Thus, if the plane of buckling is rotated to the principal plane (plane of buckling is dictated by the minimum of elastic energy after the onset of instability), the propagating shear wave of the lowest frequency in FCs deformed close to the onset of instability are polarized in the non-principal plane. In this subsection, we illustrate unit polarizations of the shear waves via the simplified scheme explained in Fig. 5. In particular, Fig. 5(a) and (b) show the first and second 3D shear wave modes propagating in FC with $b/a = 4$. The 2D images correspond to the cut planes (highlighted by red) of 3D eigenmodes. The red and green arrows in Fig. 5 represent the unit polarization vectors, which are independent of the cut plane $(X - Y)$ in the considered example. Note that the unit polarizations barely change with the cut plane $(X - Y)$ in all examples considered in this section; therefore, it is possible to illustrate them by means of the simplified scheme shown in Fig. 5(c). Thus, we investigate the in-plane modes of shear wave propagation in this work.

Fig. 6 presents dispersion curves for shear waves propagating in the direction of fibers in FCs with aspect ratio $b/a = 2$. The dispersion curves are shown for the uniaxially compressed close to the instability point (Fig. 6(a)) and undeformed (Fig. 6(b)) FCs. Since we have two characteristic lengths (a and b) in FC with rectangular arrangement of fibers, the dispersion curves of shear waves propagating along the fibers are distinct (see dotted red and dash-dotted green curves in Fig. 6) as opposite to FC with square arrangement of fibers, where the dispersion curves for two shear waves coincide (Galich, Slesarenko et al., 2017). Consistently with our previous observations for FCs with square arrays of fibers (Galich, Slesarenko et al., 2017), significant nonlinearity of dispersion curves is observed for the shear waves with wavelengths being comparable to the characteristic lengths of the FC, namely $l \sim (a + b)$. The uniaxial compression shifts dispersion curves towards lower frequencies and barely influence unit polarizations of shear waves with wavenumbers higher than certain value (e.g. $\tilde{k} > 0.2$ in Fig. 6 (a)). However, the polarizations of long shear waves ($\tilde{k} \to 0$) in the FCs compressed close to the instability point are rotated against the polarizations in the undeformed FCs (see Fig. 6(a) and (b)). This indicates that the fibers will develop buckling shapes neither in $X - Z$ nor in $Y - Z$ principal plane. Physically, fibers may buckle in the non-principal plane, because FC may be "softer/weaker" in that plane.

Remarkably, uniaxial compression along the fibers can induce pronounced nonlinearity in dispersion curves of shear waves propagating in the direction of fibers, while they are almost linear for undeformed FCs with small volume fraction of fibers. Moreover, as we increase the aspect ratio of the FC, the difference between the dispersion curves of the shear waves increases. This is illustrated by the example of the FCs with volume fraction of fibers $v_f = 0.05$ and shear modulus contrast between fibers and matrix $\mu_f/\mu_m = 15$ in Fig. 7. In particular, while the dispersion curves of two shear waves

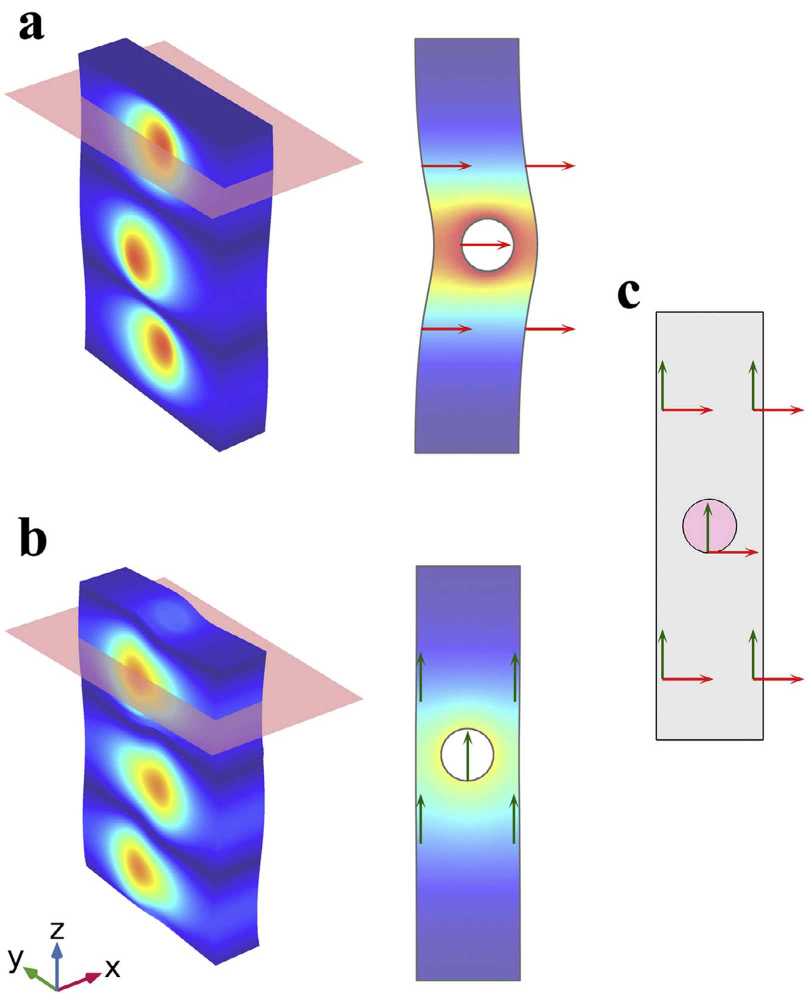

Fig. 5. An example of 3D eigenmodes and their cut planes ($X-Y$) for shear waves propagating in the direction of fibers in uniaxially compressed FC with rectangular arrays of fibers, namely $\lambda = 0.77$, $k(a+b)/(4\pi) = 0.81$, $b/a = 4$, $v_f = 0.05$, $\mu_f/\mu_m = 15$, and $\rho_f/\rho_m = 1$. (a) first eigenmode, (b) second eigenmode, (c) combined simplified scheme, where the arrows represent unit polarization vectors, which are independent of the cut plane ($X-Y$).

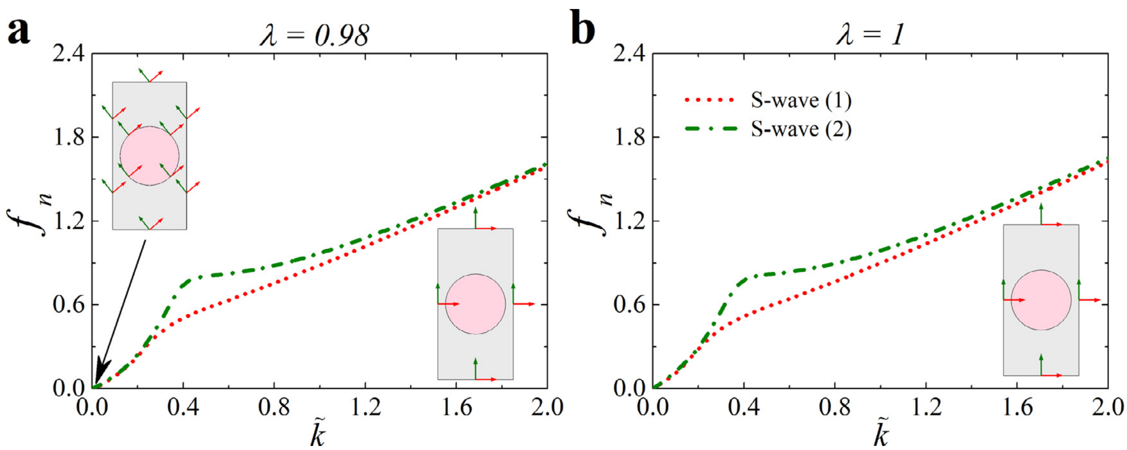

Fig. 6. Dispersion curves for shear waves propagating in the direction of fibers in FCs subjected to uniaxial deformation of (a) $\lambda = 0.98$ and (b) $\lambda = 1$ with rectangular ($b = 2a$) arrays of fibers. $v_f = 0.25$, $\mu_f/\mu_m = 100$, and $\rho_f/\rho_m = 1$. The red (green) arrows, representing unit polarization vectors, correspond to the red (green) dispersion curves. The corresponding critical stretch is $\lambda_{cr} = 0.979$. (For interpretation of the references to color in this figure legend, the reader is referred to the web version of this article.)

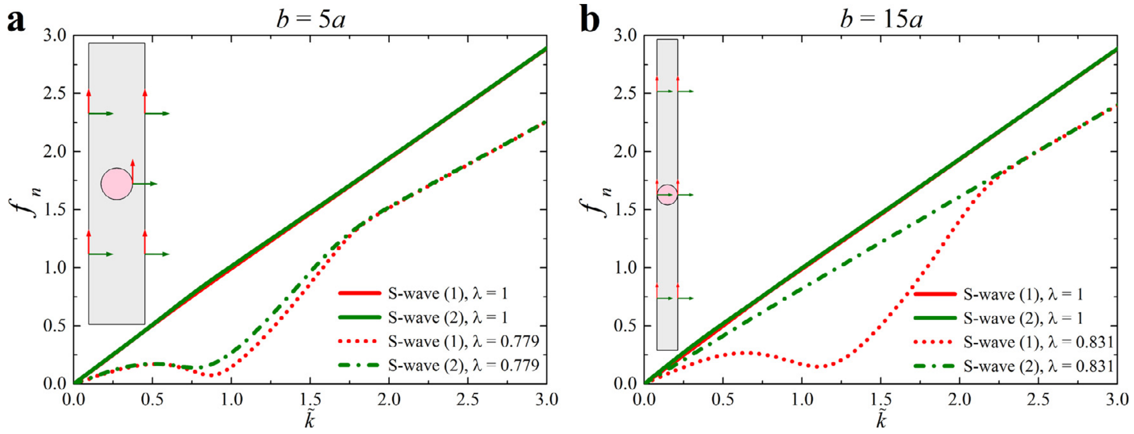

Fig. 7. Dispersion curves for shear waves propagating in the direction of fibers in undeformed and uniaxially compressed FCs with rectangular arrays of fibers, namely $b/a = 5$ (a) and $b/a = 15$ (b), $v_f = 0.05$, $\mu_f/\mu_m = 15$, and $\rho_f/\rho_m = 1$. The corresponding critical stretches for the FCs with $b/a = 5$ and $b/a = 15$ are $\lambda_{cr} = 0.778$ and $\lambda_{cr} = 0.830$, respectively.

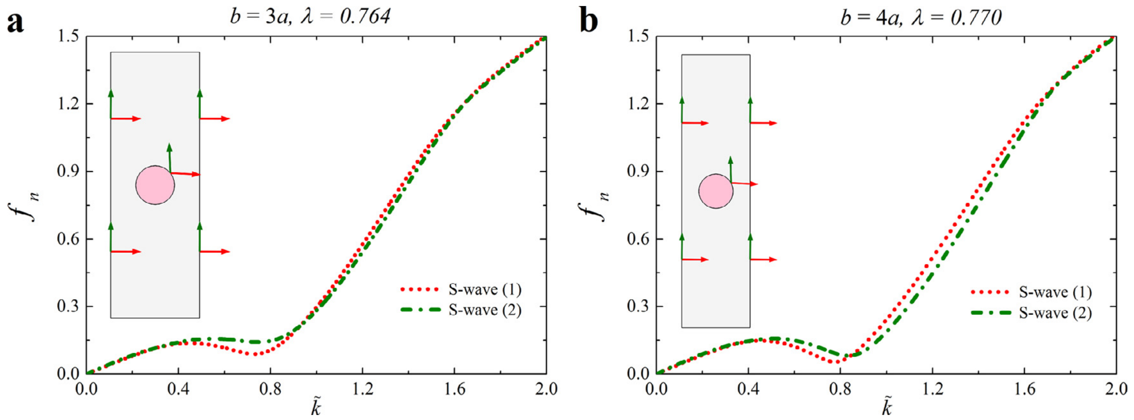

Fig. 8. Dispersion curves for shear waves propagating in the direction of fibers in uniaxially compressed FCs with rectangular arrays of fibers, namely $b/a = 3$ (a) and $b/a = 4$ (b), $v_f = 0.05$, $\mu_f/\mu_m = 15$, and $\rho_f/\rho_m = 1$. The corresponding critical stretches for the FCs with $b/a = 3$ and $b/a = 4$ are $\lambda_{cr} = 0.762$ and $\lambda_{cr} = 0.769$, respectively.

nearly coincide for the uniaxially compressed FC with aspect ratio $b/a = 5$ (compare dotted red and dash-dotted green curves in Fig. 7(a)), the dispersion curves significantly differ for the uniaxially compressed FC with aspect ratio $b/a = 15$ (compare dotted red and dash-dotted green curves in Fig. 7 (b)). Furthermore, the dispersion curves have negative slopes for some compressive stretches (see dotted red and dash-dotted green curves in Fig. 7(a) and dotted red in Fig. 7(b)), which means that the group velocities of shear waves with certain wavelengths become negative in the nearly unstable, but still stable, FC. Physically, this means that directions of energy and wave propagation are opposite to each other, because energy travels with the group velocity in periodic elastic media (Willis, 2016). Thus, shear waves with negative group velocities foreshadow the onset of elastic instability in compressed FC. Fig. 7(a) and (b) also show that the shear waves of the lowest frequencies are polarized in plane $Y - Z$ (see red arrows in Fig. 7). The latter indicates that fibers develop buckling in the plane $Y - Z$ in FCs with $b = 5a$ and $b = 15a$. According to our calculations, this holds true for FCs with $b \geq 5a$.

For the FCs with $b = 3a$ and $b = 4a$, however, the shear waves of the lowest frequencies are polarized either in plane $X - Z$ or in plane $Y - Z$ depending on the wavenumber, as shown in Fig. 8. In particular, the shear waves with wavenumber $\tilde{k} = 0.75$ and frequencies $f_n = 0.06$ and $f_n = 0.10$ are polarized in planes $X - Z$ and $Y - Z$, respectively; while the shear waves with wavenumber $\tilde{k} = 1.20$ and frequencies $f_n = 0.45$ and $f_n = 0.52$ are polarized in planes $Y - Z$ and $X - Z$, respectively (see Fig. 8(b)). This is because the dispersion curves of the shear waves intersect for these FCs. Thus, fibers start to buckle in the unexpected direction of their closest neighbors (i.e. in the plane $Z - X$) in FCs with small aspect ratios ($2a \leq b \leq 4a$), because the shear waves of the lowest frequencies in the vicinity of the critical wavenumber are polarized in plane $X - Z$ (see red arrows in Fig. 8). This is in line with the result from previous subsection, devoted to elastic instabilities of FCs with rectangular arrays, namely the FCs with large aspect ratios tend to mimic 3D laminates.

Hence, the polarizations of the shear waves with the lowest frequencies in FCs deformed close to the instability point significantly depend on the aspect ratio, regardless of the volume fraction of the fibers (compare Figs. 6–8).

5. Conclusions

We considered small-amplitude shear wave propagation in the marginally stable FCs (stable FCs brought to the vicinity of instability) with rectangular arrays of fibers. We found that shear wave propagation in direction of fibers in uniaxially compressed FCs with rectangular arrays of fibers significantly depends on the aspect ratio of the FCs. In particular, we showed that the dispersion curves of shear waves become significantly nonlinear in finitely deformed FCs with rectangular arrays of fibers, while they are almost linear in undeformed FCs with small fiber volume fractions. We also found that polarizations of shear waves having the lowest frequencies in FCs deformed close to the instability point depend on the aspect ratio, namely the shear waves with the lowest frequencies and with the wavelengths close to the critical one are polarized in planes $Z-X$ or $Z-Y$ depending on the aspect ratio of FC. As a consequence, buckling plane depends on the aspect ratio of FCs. In particular, fibers start to buckle in plane $Z-X$ for FCs with $2a \le b \le 4a$ and in plane $Z-Y$ for FCs with $5a \le b \le 15a$ if $\nu_f = 0.05$ and $\mu_f/\mu_m = 15$. However, for marginally stable FCs with large volume fraction of fibers (e.g. $\nu_f = 0.25$, $b/a = 2$ and $\mu_f/\mu_m = 15$), buckling of the fibers develop in the non-principal plane (neither $Z-X$ nor $Z-Y$), because the long shear waves are polarized in the non-principal plane. Note that although higher frequency branches exist in the system, here we consider only lower branches, the behavior of which are connected to elastic instabilities in periodic FCs. Another feature of periodic FCs is the existance of band gaps ("forbidden" frequency ranges) for certain propagation directions (Bertoldi & Boyce, 2008); however, there are no band gaps for shear waves propagating along fibers.

Finally, we found that regardless of the volume fraction and shear modulus ($\mu_f > \mu_m$) of fibers, an increase in aspect ratio of FC decreases the deformation range, where FC is stable. The critical wavenumber decreases with an increase in aspect ratio for FCs developing instability via microscopic scenario. Moreover, the compressive critical stretches leading to the onset of instability in FCs with rectangular arrays of fibers are bounded by the corresponding critical values for the 3D layered composites (upper bound) and for the FCs with square arrays of fibers (lower bound) (see Fig. 4).

Acknowledgments

The authors gratefully acknowledge the support of the Israel Science Foundation (grant 1550/15). Pavel Galich thanks the support through the Jacobs Fellowship. Viacheslav Slesarenko thanks the support through the Technion Postdoctoral Fellowship. Jian Li thanks the support of Lady Davis Fellowship.

References

Aberg, M., & Gudmundson, P. (1997). The usage of standard finite element codes for computation of dispersion relations in materials with periodic microstructure. *Journal of the Acoustical Society of America, 102*, 2007–2013. doi:10.1121/1.419652.

Agoras, M., Lopez-Pamies, O., & Castañeda, P. P. (2009). Onset of macroscopic instabilities in fiber-reinforced elastomers at finite strain. *Journal of the Mechanics and Physics of Solids, 57*, 1828–1850. doi:10.1016/j.jmps.2009.08.001.

Andrianov, I. V., Kalamkarov, A. L., & Weichert, D. (2012). Buckling of fibers in fiber-reinforced composites. *Composites Part B: Engineering, 43*(4), 2058–2062. doi:10.1016/j.compositesb.2012.01.055.

Beloshenko, V., Voznyak, Y., Voznyak, A., & Savchenko, B. (2017). New approach to production of fiber reinforced polymer hybrid composites. *Composites Part B: Engineering, 112*, 22–30. doi:10.1016/j.compositesb.2016.12.030.

Bertoldi, K., & Boyce, M. C. (2008). Wave propagation and instabilities in monolithic and periodically structured elastomeric materials undergoing large deformations. *Physical Review B, 78*, 184107. doi:10.1103/PhysRevB.78.184107.

deBotton, G., Hariton, I., & Socolsky, E. A. (2006). neo-Hookean fiber-reinforced composites in finite elasticity. *Journal of the Mechanics and Physics of Solids, 54*, 533–559. doi:10.1016/j.jmps.2005.10.001.

Galich, P. I., Fang, N. X., Boyce, M. C., & Rudykh, S. (2017). Elastic wave propagation in finitely deformed layered materials. *Journal of the Mechanics and Physics of Solids, 98*, 390–410. doi:10.1016/j.jmps.2016.10.002.

Galich, P. I., & Rudykh, S. (2017). Shear wave propagation and band gaps in finitely deformed dielectric elastomer laminates: Long wave estimates and exact solution. *Journal of Applied Mechanics, 84*(9), 091002. doi:10.1115/1.4037159.

Galich, P. I., Slesarenko, V., & Rudykh, S. (2017). Shear wave propagation in finitely deformed 3D fiber-reinforced composites. *International Journal of Solids and Structures, 110–111*, 294–304. doi:10.1016/j.ijsolstr.2016.12.007.

Gao, C., & Li, Y. (2017). Tuning the wrinkling patterns of an interfacial/coating layer via a regulation interphase. *International Journal of Solids and Structures, 104–105*, 92–102. doi:10.1016/j.ijsolstr.2016.08.003.

Geymonat, G., Müller, S., & Triantafyllidis, N. (1993). Homogenization of nonlinearly elastic materials, microscopic bifurcation and macroscopic loss of rank-one convexity. *Archive for Rational Mechanics and Analysis, 122*, 231–290. doi:10.1007/BF00380256.

Humphrey, J. D. (2002). *Cardiovascular solid mechanics: Cells, tissues, and organs*. New York: Springer-Verlag.

Kushwaha, M., Halevi, P., Dobrzynski, L., & Djafari-Rouhani, B. (1993). Acoustic band structure of periodic elastic composites. *Physical Review Letters, 71*(13), 2022–2025. doi:10.1103/PhysRevLett.71.2022.

Li, J., Slesarenko, V., Galich, P. I., & Rudykh, S. (2018). Oblique shear wave propagation in finitely deformed layered composites. *Mechanics Research Communications, 87*, 21–28. doi:10.1016/j.mechrescom.2017.12.002.

Li, Y., Kaynia, N., Rudykh, S., & Boyce, M. C. (2013). Wrinkling of interfacial layers in stratified composites. *Advanced Engineering Materials, 15*(10), 921–926. doi:10.1002/adem.201200387.

Lopez-Pamies, O., & Castañeda, P. P. (2006a). On the overall behavior, microstructure evolution, and macroscopic stability in reinforced rubbers at large deformations: I—theory. *Journal of the Mechanics and Physics of Solids, 54*, 807–830. doi:10.1016/j.jmps.2005.10.006.

Lopez-Pamies, O., & Castañeda, P. P. (2006b). On the overall behavior, microstructure evolution, and macroscopic stability in reinforced rubbers at large deformations: II—application to cylindrical fibers. *Journal of the Mechanics and Physics of Solids, 54*, 831–863. doi:10.1016/j.jmps.2005.10.010.

Merodio, J., & Ogden, R. W. (2002). Material instabilities in fiber-reinforced nonlinearly elastic solids under plane deformation. *Archives of Mechanics (IPPT), 54*, 525–552.

Merodio, J., & Pence, T. J. (2001). Kink surfaces in a directionally reinforced neo-Hookean material under plane deformation: II. Kink band stability and maximally dissipative band broadening. *Journal of Elasticity, 62*(2), 145–170. doi:10.1023/A:101169332.

Michel, J., Lopez-Pamies, O., Ponte Castañeda, P., & Triantafyllidis, N. (2010). Microscopic and macroscopic instabilities in finitely strained fiber-reinforced elastomers. *Journal of the Mechanics and Physics of Solids, 58*(11), 1776–1803. doi:10.1016/j.jmps.2010.08.006.

Nam, N., Merodio, J., Ogden, R., & Vinh, P. (2016). The effect of initial stress on the propagation of surface waves in a layered half-space. *International Journal of Solids and Structures, 88–89*, 88–100. doi:10.1016/J.IJSOLSTR.2016.03.019.

Nam, N. T., Merodio, J., & Vinh, P. C. (2016). The secular equation for non-principal Rayleigh waves in deformed incompressible doubly fiber-reinforced nonlinearly elastic solids. *International Journal of Non-Linear Mechanics, 84*, 23–30. doi:10.1016/j.ijnonlinmec.2016.04.006.

Nestorovic, M. D., & Triantafyllidis, N. (2004). Onset of failure in finitely strained layered composites subjected to combined normal and shear loading. *Journal of the Mechanics and Physics of Solids, 52*, 941–974. doi:10.1016/j.jmps.2003.06.001.

Ogden, R., & Singh, B. (2011). Propagation of waves in an incompressible transversely isotropic elastic solid with initial stress: Biot revisited. *Journal of Mechanics of Materials and Structures, 6*(1–4), 453–477. doi:10.2140/jomms.2011.6.453.

Parnes, R., & Chiskis, A. (2002). Buckling of nano-fibre reinforced composites: A re-examination of elastic buckling. *Journal of the Mechanics and Physics of Solids, 50*(4), 855–879. doi:10.1016/S0022-5096(01)00101-6.

Qiu, G., & Pence, T. (1997). Loss of ellipticity in plane deformation of a simple directionally reinforced incompressible nonlinearly elastic solid. *Journal of Elasticity, 49*, 31–63. doi:10.1023/A:1007441804480.

Rogerson, G., & Scott, N. (1994). Doubly constrained elastic wave propagation. *International Journal of Solids and Structures, 31*(20), 2769–2792. doi:10.1016/0020-7683(94)90068-X.

Rudykh, S., & deBotton, G. (2012). Instabilities of hyperelastic fiber composites: micromechanical versus numerical analyses. *Journal of Elasticity, 106*, 123–147. doi:10.1007/s10659-011-9313-x.

Saheb, D. N., & Jog, J. P. (1999). Natural fiber polymer composites: A review. *Advances in Polymer Technology, 18*(4), 351–363. doi:10.1002/(SICI)1098-2329(199924)18:4⟨351::AID-ADV6⟩3.0.CO;2-X.

Scott, N. (1991). Small vibrations of prestrained constrained elastic materials: The idealized fibre-reinforced material. *International Journal of Solids and Structures, 27*(15), 1969–1980. doi:10.1016/0020-7683(91)90189-M.

Scott, N. (1992). Waves in a homogeneously prestrained incompressible, almost inextensible, fibre-reinforced elastic material. *Proceedings of the Royal Irish Academy. Section A: Mathematical and Physical Sciences, 92A*(1), 9–36.

Scott, N., & Hayes, M. (1976). Small vibrations of a fibre-reinforced composite. *The Quarterly Journal of Mechanics and Applied Mathematics, 29*(4), 467–486. doi:10.1093/qjmam/29.4.467.

Slesarenko, V., & Rudykh, S. (2017). Microscopic and macroscopic instabilities in hyperelastic fiber composites. *Journal of the Mechanics and Physics of Solids, 99*, 471–482. doi:10.1016/j.jmps.2016.11.002.

Triantafyllidis, N., & Maker, B. N. (1985). On the comparison between microscopic and macroscopic instability mechanisms in a class of fiber-reinforced composites. *Journal of Applied Mechanics, Transactions ASME, 52*, 794–800. doi:10.1115/1.3169148.

Triantafyllidis, N., Nestorovic, M. D., & Schraad, M. W. (2006). Failure surfaces for finitely strained two-phase periodic solids under general in-plane loading. *Journal of Applied Mechanics, Transactions ASME, 73*(3), 505–515. doi:10.1115/1.2126695.

Truesdell, C., & Noll, W. (1965). *The non-linear field theories of mechanics*. Springer.

Vinh, P. C., & Merodio, J. (2013). On acoustoelasticity and the elastic constants of soft biological tissues. *Journal of Mechanics of Materials and Structures, 8*(5–7), 359–367. doi:10.2140/jomms.2013.8.359.

Vinh, P. C., Merodio, J., Hue, T. T. T., & Nam, N. T. (2014). Non-principal Rayleigh waves in deformed transversely isotropic incompressible non-linearly elastic solids. *IMA Journal of Applied Mathematics, 79*(5), 915–928. doi:10.1093/imamat/hxu023.

Willis, J. (2016). Negative refraction in a laminate. *Journal of the Mechanics and Physics of Solids, 97*, 10–18. doi:10.1016/j.jmps.2015.11.004.